# Universal and non-universal behavior in Dirac spectra

M.E. Berbenni-Bitsch[a*], M. Göckeler[b], S. Meyer[a], A. Schäfer[b], and T. Wettig[c†]

[a]Fachbereich Physik–Theoretische Physik, Universität Kaiserslautern, D-67663 Kaiserslautern, Germany

[b]Institut für Theoretische Physik, Universität Regensburg, D-93040 Regensburg, Germany

[c]Institut für Theoretische Physik, Technische Universität München, D-85747 Garching, Germany

arXiv:hep-lat/9809058v1 10 Sep 1998

We have computed ensembles of complete spectra of the staggered Dirac operator using four-dimensional SU(2) gauge fields, both in the quenched approximation and with dynamical fermions. To identify universal features in the Dirac spectrum, we compare the lattice data with predictions from chiral random matrix theory for the distribution of the low-lying eigenvalues. Good agreement is found up to some limiting energy, the so-called Thouless energy, above which random matrix theory no longer applies. We determine the dependence of the Thouless energy on the simulation parameters using the scalar susceptibility and the number variance.

## 1. Introduction

The low-energy particle spectrum implies that the chiral symmetry which the QCD Lagrangian possesses in the limit of massless quarks is spontaneously broken. The corresponding order parameter, the chiral condensate, can be related to the pion decay constant through the Gell-Mann–Oakes–Renner relation [1]. On the other hand, the chiral condensate is directly related to the density of the smallest eigenvalues of the Dirac operator via the Banks-Casher relation [2].

On the lattice, the density of the low-lying eigenvalues of the Dirac operator is strongly dependent on the choice of the fermion action. The staggered fermion action respects a chiral $\mathrm{U_A}(1)$ symmetry and, as a consequence, the nonzero eigenvalues of the Dirac operator occur in pairs $\pm\lambda_n$. Therefore, the eigenvalues near zero and in the bulk of the spectrum can be distinguished. The Wilson fermion action breaks chiral symmetry explicitly, and there is no $\mathrm{U_A}(1)$ symmetry for the hermitian Wilson Dirac operator.

In this contribution, we will be concerned with universal features in the spectrum of the staggered Dirac operator. We will mainly concentrate on the low-lying eigenvalues since they are particularly relevant for chiral symmetry breaking. The Banks-Casher relation [2], $\pi\rho(0) = V\Sigma$, relates the eigenvalue density, $\rho(\lambda) = \langle\sum_n \delta(\lambda-\lambda_n)\rangle$, of the Dirac operator at zero virtuality to the absolute value of the chiral condensate, $\Sigma$. $V$ is the four-volume. If chiral symmetry is spontaneously broken, this relation implies that the spacing of the small eigenvalues is $\sim 1/(V\Sigma)$. Since the eigenvalues of the non-interacting Dirac operator are spaced like $1/V^{1/4}$, this means that the Dirac eigenvalues in QCD must be strongly correlated.

Leutwyler and Smilga [3] derived an effective low-energy theory which is valid in the range $1/\Lambda < L < 1/m_\pi$, where $L$ is the linear extent of the box, $\Lambda$ is a typical hadronic scale, and $m_\pi$ is the pion mass. In this region, the kinetic terms in the chiral Lagrangian can be neglected, and only the symmetries are important. It was then conjectured by Shuryak and Verbaarschot [4] that the distribution of the small Dirac eigenvalues, averaged over gauge field configurations, is universal in the sense that it only depends on global symmetries of the Dirac operator. The essential ingredient is the spontaneous breaking of chiral symmetry in the QCD vacuum. Given this fact, the statistical properties of the low-lying eigenvalues can be computed in a much simpler theory, e.g., chiral random matrix theory (RMT). Alternatively, one can use the finite-volume partition function of Leutwyler and Smilga. We will not address this point since it is discussed in the con-

*Poster presented by M.E. Berbenni-Bitsch

†Talks presented by T. Wettig

tribution by P.H. Damgaard [5].

To resolve the low-lying Dirac eigenvalues, one rescales the energies by a factor of $V\Sigma$ and defines the microscopic spectral density [4],

$$\rho_s(z) = \lim_{V\to\infty} \frac{1}{V\Sigma}\rho\left(\frac{z}{V\Sigma}\right) . \quad (1)$$

This is a typical universal quantity which can be computed in chiral RMT. Other universal quantities are the distribution of the smallest eigenvalue and higher order spectral correlation functions on the microscopic scale $\lambda \sim 1/(V\Sigma)$.

We note that by concentrating on the low-lying eigenvalues, we are considering a finite-volume effect. In particular, by computing analytical results we hope to learn something about the approach to the thermodynamic limit. On the lattice, one necessarily has to perform an extrapolation to this limit. An example of the utility of the RMT results with regard to the thermodynamic limit has already been given in Ref. [6].

We briefly review chiral random matrix theory in Sec. 2 and describe numerical details of our simulations in Sec. 3. Lattice data for the small Dirac eigenvalues obtained in the quenched approximation are compared with RMT predictions in Sec. 4. New results with dynamical fermions are discussed in Sec. 5. These are particularly interesting with regard to the chiral limit. Of course, the random-matrix approach only works in a limited energy range. In Sec. 6, we will identify the domain of validity quantitatively. We conclude with a summary and an outlook to future work in Sec. 7.

## 2. Chiral random matrix theory

The Dirac operator in the continuum is defined as $D = \gamma_\mu(\partial_\mu + gA_\mu)$, where $A$ denotes the gauge field and $g$ is the coupling constant. This operator is anti-hermitian. Because of the $\mathrm{U_A}(1)$ symmetry $\{\gamma_5, D\} = 0$, all nonzero eigenvalues of $iD$ come in pairs $\pm\lambda_n$. In a chiral basis, the Dirac matrix has the structure

$$iD = \begin{bmatrix} 0 & T \\ T^\dagger & 0 \end{bmatrix} , \quad (2)$$

where $T$ is some complicated matrix. The Euclidean QCD partition function in a sector of topological charge $\nu$ is given by

$$Z^{(\nu)}_{\mathrm{QCD}} = \int \mathcal{D}A^{(\nu)} e^{-S_{\mathrm{gl}}} \prod_{f=1}^{N_f} \det(D + m_f)$$
$$= \int \mathcal{D}A^{(\nu)} e^{-S_{\mathrm{gl}}} \prod_{f=1}^{N_f} m_f^{|\nu|} \prod_{\lambda_n>0} (\lambda_n^2 + m_f^2) , \quad (3)$$

where $S_{\mathrm{gl}}$ is the gluonic action, $N_f$ is the number of quark flavors with masses $m_f$, and the $\lambda_n$ are the eigenvalues of $iD$. The superscript $(\nu)$ on $A$ means that the path integral is only over gauge fields with fixed topological charge $\nu$. The partition function is then given by $Z_{\mathrm{QCD}} = \sum_\nu e^{i\theta\nu} Z^{(\nu)}_{\mathrm{QCD}}$, where $\theta$ is the vacuum angle.

The basic idea of the random matrix approach is to substitute the matrix $T$ in Eq. (2) by a random matrix $W$, respecting the global symmetries of the problem. If the dimension of the matrix $W$ is $N \times (N + \nu)$, there are $\nu$ exact zero modes. The RMT partition function reads

$$Z^{(\nu)}_{\mathrm{RMT}} = \int \mathcal{D}W P_0(W) \prod_{f=1}^{N_f} \det(WW^\dagger + m_f^2) , \quad (4)$$

where the precise form of the distribution, $P_0(W)$, replacing $e^{-S_{\mathrm{gl}}}$ is unimportant, provided that it is invariant under rotations of $W$ and that we are interested in universal properties [7]. For convenience, one often uses a Gaussian distribution. Eventually, one is interested in the limit $N \to \infty$ which can be identified with the thermodynamic limit. The classification of the random matrix ensembles pertaining to different symmetry classes can be found in Ref. [8]. We will discuss staggered fermions with gauge group SU(2) which are described by the chiral symplectic ensemble (chSE) of RMT. In this ensemble, the elements of $W$ are real quaternions. Diagonalizing $W$ and expressing it in terms of angles and radial coordinates, the distribution of $W$ can be written as [8]

$$P(W) = P_0(W) \prod_{f=1}^{N_f} \det(WW^\dagger + m_f^2)$$
$$= P_0(\{\lambda\})\, \Delta^4(\lambda^2) \prod_n \lambda_n^{4|\nu|+3} \prod_{f=1}^{N_f} (\lambda_n^2 + m_f^2) , \quad (5)$$

where $\Delta(x) = \prod_{i>j}(x_i - x_j)$ is the Vandermonde determinant. The main mathematical problem then consists in performing integrations of this expression over all but a few variables $\lambda_n$ in the limit $N \to \infty$.

## 3. Numerical details

To check RMT predictions, one often replaces an ensemble average by a spectral average which is possible due to spectral ergodicity. Here, however, we are interested in the low-lying eigenvalues, and a spectral average is not possible. Thus, we need good statistics.

Recently, it has become feasible to calculate large ensembles of complete spectra of the staggered Dirac operator in SU(2) [9] on lattices of size up to $16^4$, extending the methods developed by Kalkreuter [10]. We determine the complete spectrum in order to make sure that the distribution of the low-lying eigenvalues has no other numerical uncertainties than the finite precision in 64 bit arithmetic.

Our numerical simulations were done on a CRAY T3E. The configurations were generated using a hybrid Monte Carlo algorithm. The boundary conditions were periodic for the gauge fields and periodic in space and anti-periodic in Euclidean time for the fermions. For the diagonalization of the Dirac matrix, we employed the Cullum-Willoughby version of the Lanczos algorithm [10]. In SU(2) with staggered fermions, every eigenvalue of $iD$ is twofold degenerate because of a global charge conjugation symmetry. In addition, the squared Dirac operator $-D^2$ couples only even to even and odd to odd lattice sites, respectively. Thus, on a lattice with $N$ sites, $-D^2$ has $N/2$ distinct eigenvalues. There is an exact sum rule for the distinct eigenvalues of $-D^2$,

$$\sum_{\lambda_n > 0} (\lambda_n a)^2 = N \,, \tag{6}$$

where $a$ is the lattice constant. Since we generated complete spectra, we could use this sum rule to check the accuracy of our eigenvalues. Equation (6) was satisfied with a relative precision of about $10^{-8}$. In Table 1, we summarize our quenched spectra. As an example, for $L = 16$ the eigenvalue spectrum has 32,768 different elements spanning four orders of magnitude. From Fig. 2 below one can read off that the fluctuations of the smallest eigenvalue cover one order of magnitude.

| $\beta$ | $L$ | # of conf. | $\langle\lambda_{\min}\rangle$ | $\tau_{\rm int}$ |
|---|---|---|---|---|
| 1.8 | 8 | 1999 | 0.00295(3) | 0.69(7) |
| 2.0 | 4 | 9979 | 0.0699(5) | 1.3(1) |
| 2.0 | 6 | 4981 | 0.0127(1) | 0.69(5) |
| 2.0 | 8 | 3896 | 0.00401(3) | 0.71(6) |
| 2.0 | 10 | 1416 | 0.00164(2) | 0.7(1) |
| 2.2 | 6 | 5542 | 0.0293(3) | 1.7(2) |
| 2.2 | 8 | 2979 | 0.0089(1) | 1.2(2) |
| 2.4 | 16 | 921 | 0.00390(9) | 1.2(3) |
| 2.5 | 8 | 576 | 0.194(9) | 8(3) |
| 2.5 | 16 | 543 | 0.016(2) | 12(7) |

Table 1
Summary of our quenched spectra with $\beta = 4/g^2$ and $V = L^4$. The last two columns represent the average value of the smallest eigenvalue (in units of $1/2a$) and its integrated autocorrelation time, respectively.

## 4. Quenched results

Our first studies were done in the quenched approximation where the fermion determinants in Eq. (5) are absent. Most of the results were reported in Refs. [9,6,11]. In Fig. 1, we show the microscopic spectral density obtained for three different sets of parameters, covering strong and weak coupling. To compare the data with the RMT prediction [Eq. (7) below with $\alpha = 0$] one needs to compute the parameter $V\Sigma$ which sets the energy scale. This parameter is determined by the data via the Banks-Casher relation, $V\Sigma = \pi\rho(0)$. [Since we have the complete spectrum for many configurations, we can easily fit $\rho(0)$]. Thus, the comparison of Fig. 1 is parameter-free.

The microscopic spectral density has an oscillatory structure. The maxima correspond roughly to the most likely positions of the individual

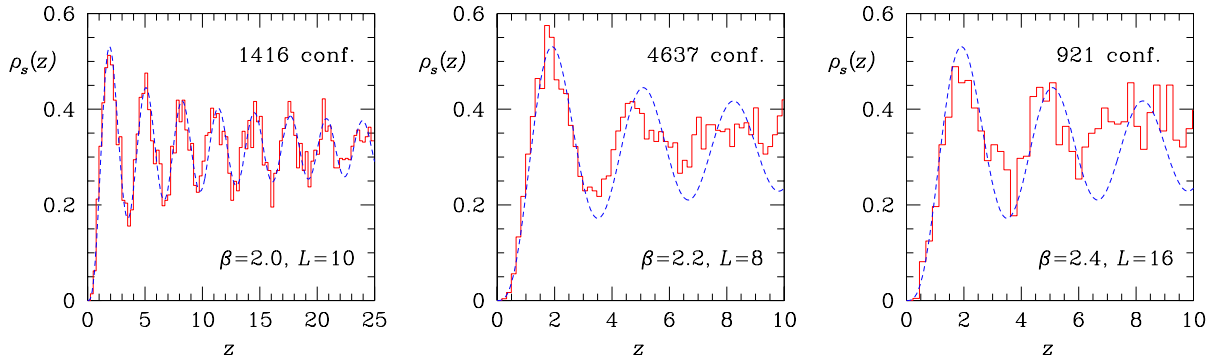


Figure 1. Microscopic spectral density of the lattice Dirac operator (histograms) and RMT prediction (dashed lines) for three different parameter sets. Lattice size $L^4$, inverse coupling constant $\beta = 4/g^2$, and number of configurations are shown in the figures.

eigenvalues. One can also compute the distribution of the smallest eigenvalue alone, or higher order spectral correlation functions. For details, we refer to Refs. [9,11].

The data agree with the RMT prediction for topological charge $\nu = 0$ (an example is shown in Fig. 2). This is due to the fact that in the derivation of the RMT results for $\nu \neq 0$, it is assumed that the Dirac operator has $|\nu|$ exact zero modes. On the lattice, the would-be zero modes (in lattice units) are shifted by an amount proportional to $a^2$. Therefore, unless $a$ is very small or some form of improvement is used, we expect to find agreement of the lattice data with the RMT results for $\nu = 0$.

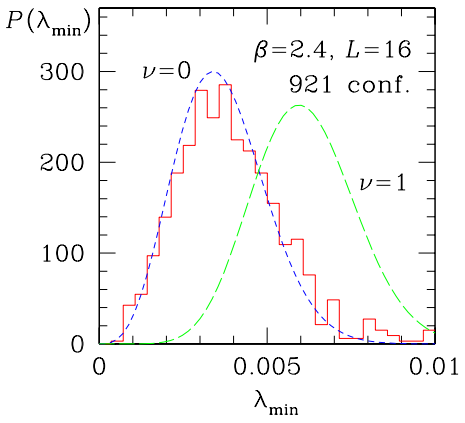


Figure 2. Distribution of the smallest eigenvalue of the lattice Dirac operator (histogram) and RMT predictions for topological sectors $\nu = 0$ (short dashes) and $\nu = 1$ (long dashes) for $\beta = 2.4$ on a $16^4$ lattice.

We can see from Fig. 1 that the agreement of the data with the RMT result breaks down at some value of the rescaled energy. The domain of validity of RMT depends on the lattice volume and on the coupling constant. A quantitative discussion of this issue will be given in Sec. 6. From the figures, one can see that the range of validity increases with increasing lattice volume and decreasing $\beta$.

## 5. Results with dynamical fermions

The results obtained in the quenched approximation are very encouraging. The natural next step is to include the fermion determinants in Eq. (5). Now an additional parameter enters the problem, the quark mass (assuming that we consider degenerate quarks). Again, we are interested in the small eigenvalues of magnitude $\sim 1/(V\Sigma)$, i.e., $z = \lambda V\Sigma \sim \mathcal{O}(1)$. From Eq. (5) it is intuitively clear that we will only see an effect of the dynamical quarks on the microscopic spectral correlations if the quark mass is also of this size. For convenience, we rescale the quark mass by the same factor as the eigenvalues and define $\mu = mV\Sigma$. For $\mu \gg 1$, we should simply

obtain results which are identical to the quenched approximation, since in this limit the fermion determinants do not affect the small eigenvalues. To observe results which are different from those obtained in the quenched approximation, we require $\mu \sim \mathcal{O}(1)$.

In the following, we summarize recent results obtained in Ref. [12]. Analytical RMT results for the microscopic spectral density in the presence of massive dynamical quarks are currently only known for the unitary (UE) and chiral unitary (chUE) ensemble [13]. For the chSE, results are known in the chiral limit. We have [14,6,11]

$$\rho_s(z) = z[J_\alpha^2(2z) - J_{\alpha+1}(2z)J_{\alpha-1}(2z)] - \frac{1}{2}J_\alpha(2z)\int_0^{2z} dt J_\alpha(t)\,, \qquad (7)$$

where $\alpha = N_f + 2|\nu|$ and $J$ denotes the Bessel function. If $\alpha$ is zero or an odd integer, RMT results for the distribution of the smallest eigenvalue are known analytically [15,16]. For even $\alpha \neq 0$ (this is relevant in our case), they can be obtained as an expansion in zonal polynomials [17,12]. For $\mu \neq 0$, the RMT results for $\rho_s(z)$ and $P(\lambda_{\rm min})$ can be obtained numerically by constructing skew-orthogonal polynomials which obey orthogonality relations determined by a weight function involving the fermion determinants [14,12]. To avoid cancellation problems, a multi-precision package was used [18].

Some of our numerical results are shown in Figs. 3 and 4. In this first exploratory study, we chose values of $\beta$ in the strong-coupling region since there one does not need very large lattices to obtain agreement with RMT, see the end of Sec. 4 and Sec. 6. The RMT results were computed with $\nu = 0$ for the reason discussed in Sec. 4. Again, there is only one parameter, $V\Sigma$, which sets the energy scale and is determined by the data from the Banks-Casher formula. We have also plotted the RMT results for $\rho_s(z)$ and $P(\lambda_{\rm min})$ in the quenched approximation and in the chiral limit, respectively. The data should agree with these two curves in the limits $\mu \gg 1$ and $\mu = 0$, respectively. For $\mu \sim \mathcal{O}(1)$, the data should lie somewhere in between these two limiting curves. This is indeed observed in the figures.

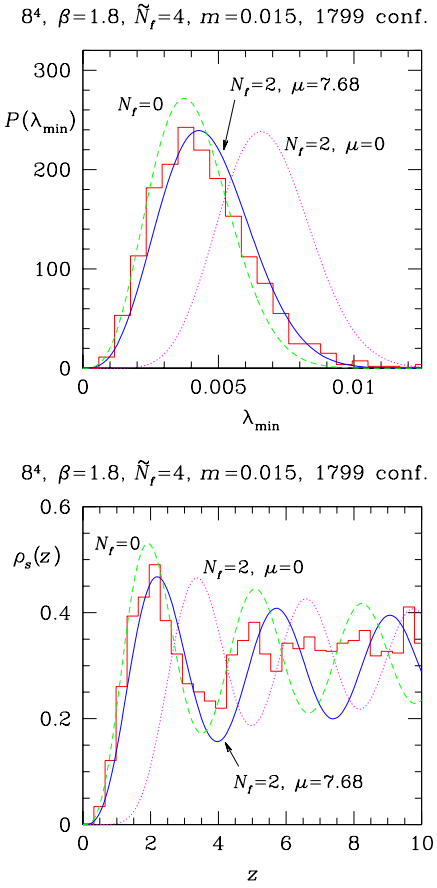


Figure 3. Distribution of the smallest eigenvalue (top) and microscopic spectral density (bottom) for the simulation parameters indicated above the figures. The histograms represent the lattice data. The solid curves are the RMT results computed with the appropriate value of the rescaled quark mass $\mu$. The dashed and the dotted curves are the RMT results computed in the quenched approximation and in the chiral limit, respectively.

An important remark is in order. We are comparing lattice data computed with $n$ copies of staggered flavors (corresponding to $\tilde{N}_f = 4n$ flavors in the continuum limit) with RMT results computed for $N_f$ flavors, where $N_f = \tilde{N}_f/2$. This is not an ad-hoc prescription but justified by the

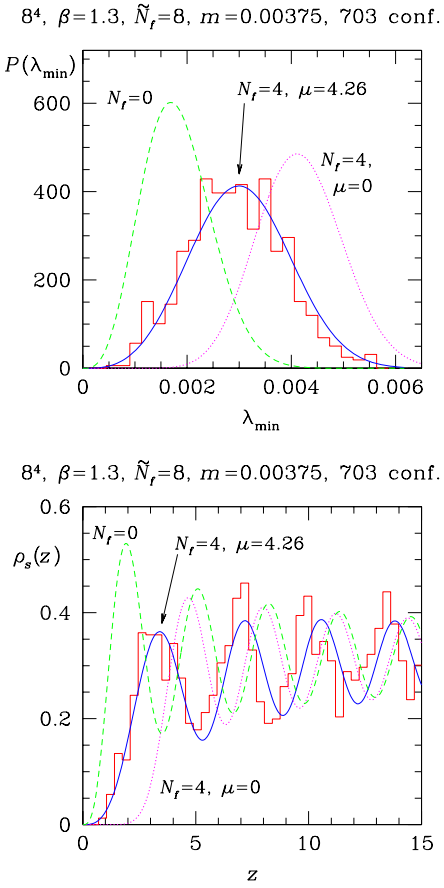


Figure 4. Same as Fig. 3 but for different simulation parameters (indicated above the figures).

combination of the following two reasons. First, the U(4)×U(4) symmetry of the continuum action (for $\tilde{N}_f = 4$) is broken to U(1)×U(1) at finite lattice spacing $a$. This would suggest to use $N_f = \tilde{N}_f/4$ in the RMT results. Second, all eigenvalues of $D$ are doubly degenerate in SU(2). However, in Eq. (5) the eigenvalues are assumed to be non-degenerate [8]. This would suggest to use $N_f = 2\tilde{N}_f$ in the RMT results. Combining the two factors, we conclude that we have to use $N_f = \frac{1}{4} \cdot 2 \cdot \tilde{N}_f = \tilde{N}_f/2$ in the RMT results.

Note that in the regime $\mu \sim \mathcal{O}(1)$, the quark mass is very small, and lattice simulations are very demanding. Testing the RMT predictions required a substantial numerical effort. However, the point is that, once the validity of the RMT description is established, the availability of analytical results for very small quark mass should facilitate extrapolations to the chiral limit which are otherwise difficult to perform on the lattice.

## 6. Crossover to non-universal behavior

As indicated above, the domain of validity of the random matrix description is finite. After all, QCD is a complicated theory and not just a random matrix model. If one wants to make practical use of the RMT results, one should know quantitatively in which energy range they apply. In condensed matter physics, the energy up to which the RMT description is valid is called the Thouless energy, $E_c$. Essentially, $E_c$ is the inverse of the diffusion time of an electron through a disordered mesoscopic sample. It behaves like $E_c \sim L^{-2}$, where $L$ is the length of the sample. Recently, some progress was made in identifying the equivalent of the Thouless energy in QCD [19–23]. Again, we shall concentrate on the low-lying eigenvalues.

The starting point is the condition for the applicability of the Leutwyler-Smilga effective theory,

$$L < \frac{1}{m_\pi}\,, \tag{8}$$

which also sets the domain of validity of the RMT description. From the Gell-Mann–Oakes–Renner relation, we have

$$m_\pi^2 f_\pi^2 = 2m\Sigma\,. \tag{9}$$

Here, $m$ is to be regarded as a valence quark mass which sets the energy scale below which RMT applies. Denoting the QCD equivalent of the Thouless energy by $\lambda_{\rm RMT}$, one obtains [20,21]

$$\lambda_{\rm RMT} \sim \frac{f_\pi^2}{\Sigma L^2}\,. \tag{10}$$

To have a dimensionless quantity, it is useful to divide $\lambda_{\rm RMT}$ by the mean level spacing at $\lambda = 0$, $\Delta = 1/\rho(0) = \pi/(V\Sigma)$. This yields

$$\lambda_{\rm RMT}/\Delta \sim \frac{1}{\pi} f_\pi^2 L^2\,. \tag{11}$$

This is the prediction which we want to test. It was already checked in the instanton liquid model and confirmed qualitatively [21]. Since we have a large number of complete spectra at our disposal, we are in a position to perform a comprehensive quantitative test against lattice data. For simplicity, we only use the quenched data. In the following, we summarize results obtained in Ref. [22].

A convenient quantity to consider in this respect is the disconnected chiral susceptibility. It is defined in terms of the Dirac eigenvalues by

$$\chi^{\rm disc}_{\rm lattice} = \frac{1}{N}\left\langle \sum_{k,l=1}^{N} \frac{1}{(i\lambda_k+m)(i\lambda_l+m)} \right\rangle - \frac{1}{N}\left\langle \sum_{k=1}^{N} \frac{1}{i\lambda_k+m} \right\rangle^2 , \qquad (12)$$

where $N = Va^{-4}$ is the number of lattice sites and $m$ is the valence quark mass. Going over to the microscopic limit, i.e., rescaling all energies by $V\Sigma$ and defining $u = mV\Sigma$, the susceptibility can be expressed in terms of the microscopic spectral one- and two-point functions. Inserting the RMT results of the chSE for these quantities and performing some tedious algebra, we obtain the RMT prediction

$$\chi^{\rm disc}_{\rm RMT} = 4u^2 \int_0^1 ds\, s^2 K_0(2su) \int_0^1 dt\, I_0(2stu) \times \Big\{ s(1-t^2) - 8st I_0(2stu) K_0(2su) + 4K_0(2u)\left[ I_0(2su) + tI_0(2stu) \right] \Big\} - 4u^2 K_0^2(2u) \left[ \int_0^1 ds\, I_0(2su) \right]^2 , \qquad (13)$$

where $I$ and $K$ denote modified Bessel functions. Note that in going from Eq. (12) to Eq. (13), $\chi^{\rm disc}$ has been rescaled by $1/(N\Sigma^2)$ to eliminate the dependence on $\beta$. The RMT result should agree with the lattice result up to some limiting value $u_{\rm RMT}$. To identify this value, it is useful to define the ratio

$$\text{ratio} = \frac{\chi^{\rm disc}_{\rm lattice} - \chi^{\rm disc}_{\rm RMT}}{\chi^{\rm disc}_{\rm RMT}} . \qquad (14)$$

Deviations of this ratio from zero indicate the breakdown of the RMT description. The ratio is plotted in Fig. 5 for one particular data set. The deviations of the ratio from zero for very small values of $u$ are artifacts of finite statistics which are explained in Ref. [22]. We are interested in the deviations from zero which set in at $u \approx 5 \sim 10$. Let us denote this value of $u$ by $u_{\rm RMT}$. It is related to $\lambda_{\rm RMT}$ by $u_{\rm RMT} = \lambda_{\rm RMT} V\Sigma = \pi\lambda_{\rm RMT}/\Delta$.

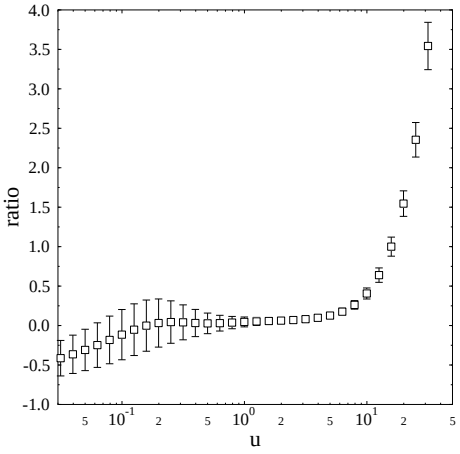


Figure 5. The ratio defined in Eq. (14) versus $u$ for the data obtained on a $10^4$ lattice using $\beta = 2.0$.

According to Eq. (11), $u_{\rm RMT}$ should scale with $L^2$. This prediction is tested in Fig. 6 where we have plotted data for four different lattice sizes at constant $\beta$ versus $u/L^2$. All data fall on the same curve, except for the deviations at small $u$ which are due to the finiteness of our statistical ensembles. This confirms the prediction that $u_{\rm RMT}$ scales with $L^2$.

It remains to test the predicted scaling with $f_\pi^2$. In order to determine $f_\pi$, we use a result of Ref. [24] where it was found that $f_\pi^2 \approx 3.4\Sigma$ in lattice units in the range of $\beta$ we consider. This suggests to plot the ratio of Eq. (14) versus $u/(\Sigma L^2)$ which we have done in Fig. 7. Again, the data fall approximately on the same curve, in particular the data for $\beta = 2.0$ and $\beta = 2.4$. (One can only expect an agreement on the level to which the relation between $f_\pi^2$ and $\Sigma$ is known.) Putting

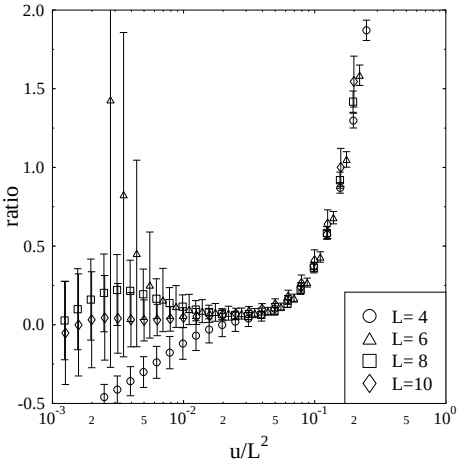


Figure 6. The ratio of Eq. (14) versus $u/L^2$ for constant $\beta = 2.0$ and four different lattice sizes $V = L^4$.

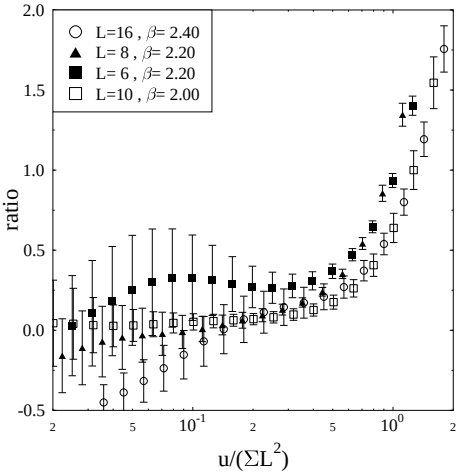


Figure 7. The ratio of Eq. (14) versus $u/(\Sigma L^2)$ for four different parameter sets.

in the numbers, we obtain

$$\lambda_{\rm RMT}/\Delta \approx 0.3 f_\pi^2 L^2 \tag{15}$$

which is in good agreement with the prediction of Eq. (11).

Another interesting quantity is the number variance in an interval $I = [0, S]$, defined by $\Sigma^2(I) = \langle (N(I) - \langle N(I)\rangle)^2\rangle$. (This $\Sigma^2$ should not be confused with the absolute value of the chiral condensate.) Here, $N(I)$ is the number of eigenvalues in $I$, and $\langle\cdots\rangle$ denotes an ensemble average. The number variance can be computed in RMT, and the lattice data agree with the RMT result up to some limiting value of $S$ which we will denote by $S_{\rm RMT}$. Considering a number of different lattice sizes and $\beta$-values we found that $S_{\rm RMT}$ scales with $f_\pi^2$ and $L^2$ as expected. Quantitatively,

$$S_{\rm RMT} \approx (0.3 \sim 0.7) f_\pi^2 L^2 \tag{16}$$

which is consistent with $u_{\rm RMT}$.

We conclude this section with the statement that the domain of validity of the RMT description of the low-lying Dirac eigenvalues in QCD is now known quantitatively. The implications of this result will be discussed in the next section.

## 7. Summary and outlook

We now have solid numerical evidence that the distribution of the low-lying Dirac eigenvalues is universal and described by RMT results, both in the quenched approximation and with dynamical fermions. Furthermore, we have a quantitative criterion for the domain of validity of the random matrix description which was confirmed by lattice simulations. How can we make practical use of this knowledge?

One point concerns extrapolations to limits that are difficult to take on the lattice. The first example is the thermodynamic limit. Since we are dealing with finite-volume effects, we can make analytical statements about how this limit is approached. This was already demonstrated in Ref. [6]. The second example is the chiral limit. We have RMT results for the microscopic spectral quantities in the presence of dynamical quarks with arbitrarily small masses. For quantities that are sensitive to the small eigenvalues, these results should provide guidance for extrapolations to the chiral limit. Third, we have the continuum limit. It is less clear in what way the random matrix approach might help in approaching this limit. One observation is that as $a \to 0$, there should be a transition in the effective number of

flavors used in the RMT results with dynamical fermions, from $\tilde{N}_f/2$ to $2\tilde{N}_f$. Presumably, $a$ has to be very small to see such a transition.

As far as topology is concerned, RMT can determine the microscopic spectral quantities only for fixed topological charge $\nu$. The overall result for some quantity will be a weighted average over all topological sectors, and RMT cannot predict the weights. So far, all data were consistent with $\nu = 0$ in the RMT results since the latter are only sensitive to exact zero modes of the Dirac operator. It would be very interesting to identify the would-be zero modes. For this, one needs the eigenvectors corresponding to the small eigenvalues. We are currently trying to compute these as well.

Last but not least, we feel that the analytical knowledge of the distribution of the smallest eigenvalues may have an impact on fermion algorithms. This is suggested by the fact that the magnitude of the small eigenvalues determines the performance of the fermion algorithm. While RMT cannot say anything about individual configurations, it predicts the statistical distribution of the small eigenvalues. This knowledge may be useful to construct more effective algorithms.

**Acknowledgments.** This work was supported in part by DFG grants Me 567/5-3 and We 655/15-1. The numerical simulations were done on a CRAY T3E-900 at the HLRS Stuttgart. We thank the MPI für Kernphysik, Heidelberg, for hospitality and support.

## REFERENCES

1. M. Gell-Mann, R.J. Oakes, and B. Renner, Phys. Rev. 175 (1968) 2195.
2. T. Banks and A. Casher, Nucl. Phys. B 169 (1980) 103.
3. H. Leutwyler and A.V. Smilga, Phys. Rev. D 46 (1992) 5607.
4. E.V. Shuryak and J.J.M. Verbaarschot, Nucl. Phys. A 560 (1993) 306.
5. P.H. Damgaard, Phys. Lett. B 424 (1998) 322 and hep-lat/9808035.
6. M.E. Berbenni-Bitsch, A.D. Jackson, S. Meyer, A. Schäfer, J.J.M Verbaarschot, and T. Wettig, Nucl. Phys. B (Proc. Suppl.) 63A-C (1998) 820.
7. G. Akemann, P.H. Damgaard, U. Magnea, and S. Nishigaki, Nucl. Phys. B 487 (1997) 721.
8. J.J.M. Verbaarschot, Phys. Rev. Lett. 72 (1994) 2531.
9. M.E. Berbenni-Bitsch, S. Meyer, A. Schäfer, J.J.M Verbaarschot, and T. Wettig, Phys. Rev. Lett. 80 (1998) 1146,
10. T. Kalkreuter, Phys. Rev. D 51 (1995) 1305.
11. J.-Z. Ma, T. Guhr, and T. Wettig, Eur. Phys. J. A 2 (1998) 87.
12. M.E. Berbenni-Bitsch, S. Meyer, and T. Wettig, hep-lat/9804030, Phys. Rev. D (in press).
13. P.H. Damgaard and S.M. Nishigaki, Nucl. Phys. B 518 (1998) 495, Phys. Rev. D 57 (1998) 5299; T. Wilke, T. Guhr, and T. Wettig, Phys. Rev. D 57 (1998) 6486.
14. T. Nagao and P.J. Forrester, Nucl. Phys. B 435 (1995) 401.
15. P.J. Forrester, Nucl. Phys. B 402 (1993) 709.
16. T. Nagao and P.J. Forrester, Nucl. Phys. B 509 (1998) 561.
17. J. Kaneko, SIAM J. Math. Anal. 24 (1993) 1086.
18. D.H. Bailey, *A Fortran-90 based multiprecision system*, NASA Ames RNR Technical Report RNR-94-013.
19. J. Stern, hep-ph/9801282.
20. R.A. Janik, M.A. Nowak, G. Papp, and I. Zahed, Phys. Rev. Lett. 81 (1998) 264.
21. J.C. Osborn and J.J.M. Verbaarschot, Phys. Rev. Lett. 81 (1998) 268, Nucl. Phys. B 525 (1998) 738.
22. M.E. Berbenni-Bitsch, M. Göckeler, T. Guhr, A.D. Jackson, J.-Z. Ma, S. Meyer, A. Schäfer, H.A. Weidenmüller, T. Wettig, and T. Wilke, hep-ph/9804439, Phys. Lett. B (in press).
23. T. Guhr, J.-Z. Ma, S. Meyer, and T. Wilke, hep-lat/9806003.
24. A. Billoire, R. Lacaze, E. Marinari, and A. Morel, Nucl. Phys. B 251 (1985) 581.